

¹ IAMAP: Unlocking Deep Learning in QGIS for non-coders and limited computing resources

³ Paul Tresson  ^{1¶}, Pierre Le Coz^{1,2}, Hadrien Tulet¹, Anthony Malkassian  ³, and Maxime Réjou-Méchain  ^{1,2}

⁵ 1 AMAP, Univ. Montpellier, IRD, CNRS, CIRAD, INRAE, Montpellier, France 2 Forest Restoration
⁶ Research Unit, Department of Biology, Faculty of Science, Chiang Mai University, Chiang Mai, Thailand
⁷ 3 Université de la Réunion, UMR PVBMT, St. Pierre, La Réunion, France ¶ Corresponding author

DOI: [10.xxxxxx/draft](https://doi.org/10.xxxxxx/draft)

Software

- [Review](#) 
- [Repository](#) 
- [Archive](#) 

Editor: 

Submitted: 01 December 2025

Published: unpublished

License

Authors of papers retain copyright and release the work under a Creative Commons Attribution 4.0 International License ([CC BY 4.0](#))¹⁹

⁸ Summary

⁹ 1. Remote sensing has entered a new era with the rapid development of artificial intelligence
¹⁰ approaches. However, the implementation of deep learning has largely remained restricted to
¹¹ specialists and has been impractical because it often requires (i) large reference datasets for
¹² model training and validation; (ii) substantial computing resources; and (iii) strong coding
¹³ skills.

¹⁴ 2. Here, we introduce IAMAP, a user-friendly QGIS plugin that addresses these three challenges
¹⁵ in an easy yet flexible way. IAMAP builds on recent advancements in self-supervised learning
¹⁶ strategies, which now provide robust feature extractors, often referred to as foundation models.
¹⁷ These generalist models can often be reliably used in few-shot or zero-shot scenarios (*i.e.*, with
¹⁸ little to no fine-tuning).

¹⁹ 3. IAMAP's interface allows users to streamline several key steps in remote sensing image
²⁰ analysis: (i) extracting image features using a wide range of deep learning architectures; (ii)
²¹ reducing dimensionality with built-in algorithms; (iii) performing clustering on features or
²² their reduced representations; (iv) generating feature similarity maps; and (v) calibrating and
²³ validating supervised machine learning models for prediction.

²⁴ 4. By enabling non-AI specialists to leverage the high-quality features provided by recent deep
²⁵ learning approaches without requiring GPU capacity or extensive reference datasets, IAMAP
²⁶ contributes to the democratization of computationally efficient and energy-conscious deep
²⁷ learning methods.

²⁸ **Keywords:** Remote sensing, Self-supervised learning, Foundation models, Machine learning,
²⁹ Artificial Intelligence, Consumer hardware.

³⁰ Statement of need

³¹ The integration of remote sensing data with deep learning approaches is currently revolutionizing
³² Earth observation sciences, leading to significant qualitative and quantitative improvements
³³ in large-scale predictions ([Yasir et al., 2023](#); [Yuan et al., 2020](#); [Zhu et al., 2017](#)). However,
³⁴ this revolution comes with a number of challenges. First, over the past decade, most deep
³⁵ learning applications have been highly data-demanding, requiring extensive manual labeling
³⁶ with typically more than one hundred thousands labeled points ([Safanova et al., 2023](#)). In
³⁷ most ecological and environmental science studies, constructing such a large reference dataset,
³⁸ through *e.g.*, ground observations or photo-interpretation, remains a major barrier to the
³⁹ implementation of deep learning approaches. Second, a common obstacle to the adoption of
⁴⁰ deep learning is the computing power required to train a model. Training a deep learning model

is indeed highly resource-intensive, primarily due to the backpropagation step (see Goodfellow, 2016). As a result, modern deep learning architectures are virtually impossible to train without substantial local Graphics Processing Unit (GPU) capacity or access to high-end computing clusters. Last but not least, implementing deep learning approaches typically requires at least basic coding skills, which has so far restricted their use to users with a minimal background in computer science.

The recent development of self-supervised learning (SSL) approaches is a game-changer in the deep learning domain, as exemplified by the success of models like BERT and ChatGPT in natural language processing (Achiam et al., 2023; Devlin, 2018). In SSL, the model starts by learning features describing a dataset via a pretext task that does not require a label. In computer vision, several SSL strategies have been proposed, typically belonging to two main categories: contrastive or generative learning. In contrastive learning, several networks view transformed versions of the same data and have to learn to produce robust representation of this data (e.g. DINOv2 (Oquab et al., 2023) or VicReg (Bardes et al., 2021)). In generative learning, a network sees a degraded version of the data (typically, a masked version) and has to learn to generate a non-degraded version (e.g., MAE, (He et al., 2022)) (for an overview of main SSL approaches, see Shwartz Ziv & LeCun, 2024). Once pre-trained on a large set of images, which remains very data- and resource-intensive, the resulting backbone can be referred to as a "foundation model". Like any pre-trained model, this foundation model can then be fine-tuned with a limited number of manually labeled examples to learn a specific downstream task (e.g. land cover classification or change detection in remote sensing) (Ericsson et al., 2021). The main difference between a pre-trained self-supervised learning (SSL) model and a pre-trained supervised model lies in their training objectives: SSL models are not constrained by predefined labels and are therefore free to explore and encode the intrinsic structure and diversity of the data, often resulting in more general and transferable representations. In contrast, supervised models are explicitly optimized to perform a specific user-defined task, which can lead to highly specialized representations that may overlook other meaningful features in the data. As such, SSL foundation models can perform well even in low-shot or zero-shot tasks, *i.e.* using the model as is, with few or no training data. Consequently, SSL models are considered particularly promising for remote sensing tasks, as demonstrated by recent works and initiatives (Cong et al., 2023; Jakubik et al., 2023; Marsocci et al., 2024; Xiong et al., 2024).

In parallel, to the development of SSL, Vision Transformers (ViT) (Dosovitskiy et al., 2020) and their derivatives (such as EVA (Fang et al., 2023) or Hiera (Ryali et al., 2023)) have changed the state of the art of computer vision. In a ViT, an image is analyzed by patches (usually 16×16 or 14×14 pixels). Each patch is projected in an embedding space and the embedding spaces of the different patches update each-others through the self-attention mechanism (see Vaswani, 2017). These architectures present the advantage that the features produced at patch level can be analyzed spatially within an image, which is relevant in remote sensing especially when working at high resolution, (see (Marsocci et al., 2024)) (see the plugin documentation for a more detailed overview of the functioning of a ViT).

With the democratization of deep learning, some developers have already worked on the integration of deep learning models in geographic information systems such as the open-source and widely used QGIS software (QGIS Development Team, 2025). However, at the time of writing, these solutions mostly focus on fine-tuning models or using a model in inference only (e.g. see Aszkowski et al., 2023; Zhao et al., 2023). Then, they are only usable by users with access to high-end computing power, extensive dataset, on interested in a task for which a specific model was already trained.

In this paper, we introduce a new plugin for QGIS designed to streamline remote sensing image analysis using advanced pre-trained deep learning models without the need for coding or extensive computing resources. As demonstrated in this paper, users can apply a pre-trained model to generate high-quality features at the patch level. The plugin then allows users to manipulate these features using various projections, clustering, similarity, and supervised machine learning (ML) algorithms.

94 Plugin description

95 The IAMAP plugin integrated into QGIS consists of five main modules, which can be used
 96 individually or sequentially on a georeferenced raster image (Fig. [Figure 1](#). We here below
 97 describe the functionality of each module.

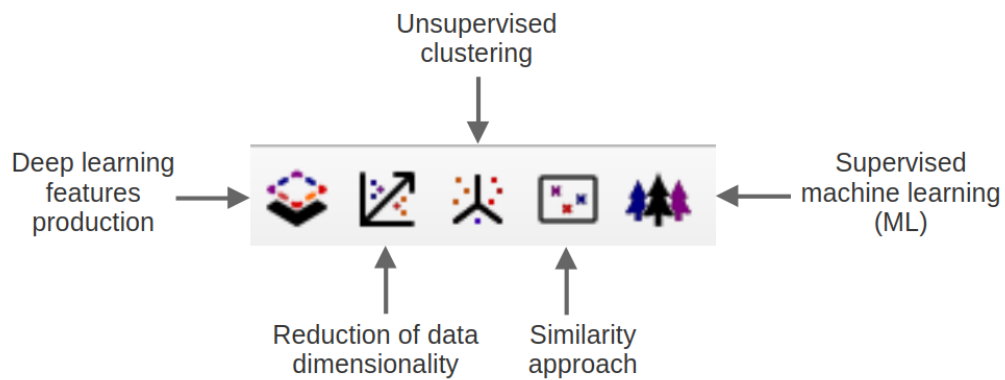


Figure 1: The five main modules of the IAMAP plugin.

98 Deep Learning feature production

99 The first and most original module of IAMAP is the deep learning feature extraction module.
 100 Using a georeferenced raster as input (a QGIS raster layer or a raster saved on disk), this
 101 module enables the use of various pre-trained deep learning models to produce a set of features
 102 describing the input raster. The use of deep learning model in inference only removes the
 103 costly training step and greatly reduce the computational power required. This module mostly
 104 relies on two widely used *pytorch* libraries: *timm* ([Wightman, 2019](#)), for loading pre-trained
 105 model weights, and *torchgeo* ([Stewart et al., 2022](#)), for handling geospatial data.

106 The *timm* library has become a standard for sharing and loading pre-trained weights in *pytorch*
 107 and is now integrated into the [HuggingFace Hub](#) ([Wolf, 2019](#)). Originally developed for sharing
 108 natural language processing (NLP) models, the HuggingFace Hub has since become the largest
 109 repository of pre-trained deep learning models, with over 400,000 models available at the
 110 time of writing. Our aim in choosing this back-end is to rely on libraries that are widely
 111 used, well maintained, and actively updated. Hence, while we propose a couple of widely used
 112 foundation models by default, the user can select any model available on HuggingFace by
 113 entering the architecture name (although not all models are guaranteed to work depending
 114 on their architecture). The plugin interface also gives the possibility to load local pre-trained
 115 models weights, if a correct *timm* architecture is chosen.

116 Handling remote sensing datasets differs from working with typical image collections used in
 117 classical computer vision. Raster images are often several orders of magnitude larger and must
 118 be sampled to fit the input requirements of neural networks, which typically expect square
 119 images a few hundred pixels wide. Additionally, it is essential to preserve the geographical
 120 metadata associated with each raster. The *torchgeo* library provides an efficient solution to
 121 address these constraints, but it includes many features and dependencies that are not all useful
 122 for our purposes. Therefore, we have forked only the necessary parts of the *torchgeo* code into
 123 our plugin. Our goal is to keep the codebase simple and minimize unnecessary dependencies.

124 The module offers several options to the user, most of which come with proposed default
 125 values. Among these, the sampling size and the stride are key parameters: the sampling size
 126 determines the dimensions of the extracted tiles while the stride controls the spacing between
 127 tiles and thus the degree of overlap used to reduce tiling artifacts. The combination of sampling

128 size, stride and the architecture chosen as encoder will determine the resolution of the output
129 raster. It is possible as well to set an overlap between tiles to reduce possible tiling effects.
130 These parameters are essential to consider, as they directly influence the trade-off between
131 model performance and inference cost.

132 The output of this module is a raster with a coarser resolution than the input raster, depending
133 on the sampling parameters and the chosen deep learning architecture. It contains as many
134 bands as the number of extracted features (e.g. 768 for a ViT-base model). By default, QGIS
135 loads the raster at the end of the process and displays only the first three bands using a
136 false-color RGB composition, although these bands are not necessarily the most informative
137 (see top row of Fig. [Figure 2](#)).

138 Computer vision state of the art pretrained models are usually trained with Red Green and Blue
139 (RGB) bands used in natural images. We thus propose three strategies for users who want to
140 work with input rasters with a band number different from 3, as it is usually the case in remote
141 sensing. One potential solution requires manipulations of the pre-trained weights to handle
142 the exact number of bands of the raw image by either copying the weights of the first layer
143 modulo 3 if the number of input bands is larger than three or averaging weights if the number
144 of input bands is smaller than three. This option should be taken with caution given that it is
145 expected to change the behavior of the model, even if it should keep a capacity for abstraction
146 and projecting low level information into a richer feature space (see Fig. [Figure 2](#) examples).
147 The second solution consists in selecting only 3 relevant bands in the deep learning module
148 without modifying the model's weights. The last option, which appears to be the most robust
149 one according to our tests, consists in applying first a dimension reduction (see next section),
150 such as a PCA, and use three reduction axes as an input in the deep learning encoder.

151 As the state of the art is evolving for remote sensing application, we also provide inference with
152 foundation models trained specifically on remote sensing data, such as DOFA ([Xiong et al.,
153 2024](#)) and a ViT pretrained on the SSL4EO dataset ([Wang et al., 2022](#)) using Marsocci et al.
154 implementation ([Marsocci et al., 2024](#)). For the DOFA encoder, multispectral bands
155 are handled by the model without manipulation of the encoder or pre-processing required.

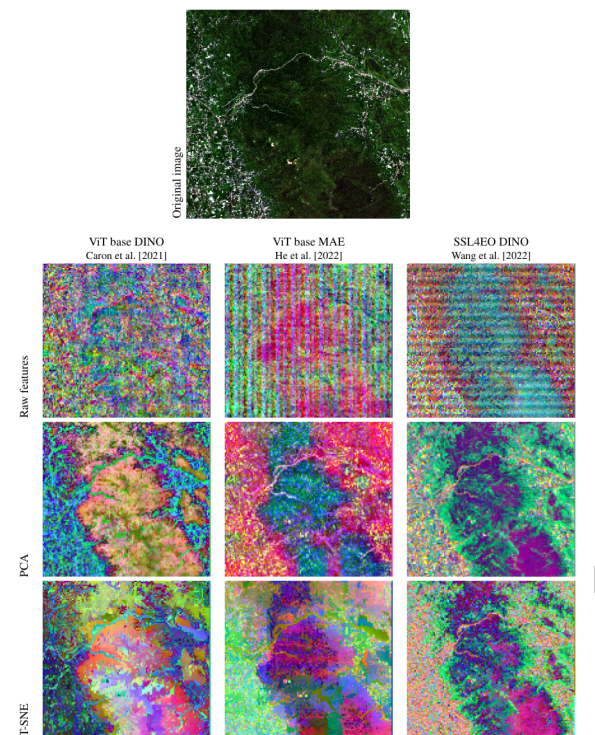


Figure 2: A sentinel 2 image of a forested landscape in Thailand (Khao Banthat Wildlife Sanctuary; Lat 7.53°, Lon 99.82°) processed by different backbones. The top row represents the first three feature dimensions output by the models (which may not be the most informative). The second row shows a 3D PCA of the features mapped to the red, green and blue channel respectively. The third row shows a projection using a 3D T-SNE.

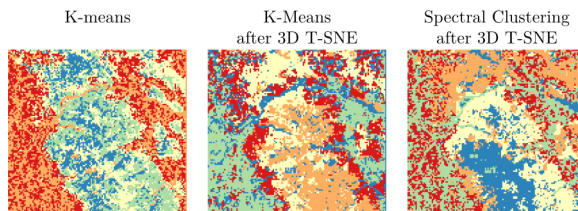
156 Reduction of data dimensionality

157 This module enables dimensionality reduction of an input raster using a variety of approaches,
 158 including PCA, t-SNE ([Van der Maaten & Hinton, 2008](#)), and UMAP ([McInnes et al., 2018](#)).
 159 This dimensionality reduction step is particularly useful for two tasks: (1) reducing the number
 160 of bands in a raw multi-band raster before applying a deep learning model, as discussed in
 161 the previous section, and (2) reducing the dimensionality of the feature space to facilitate
 162 visualization and support more robust training procedures. Indeed, deep learning models
 163 typically produce a high-dimensional feature space. While this high dimensionality poses no
 164 issues when fed into a deep learning head, it can become a drawback for visualizing the feature
 165 space and using it in lighter machine learning models such as Random Forests. To address
 166 this, it is common in deep learning research to use dimensionality reduction algorithms to
 167 visualize and analyze the feature space of a model. These reduced features can often be more
 168 informative at first glance (see the second row of Fig. [Figure 2](#)), and reducing or ordering the
 169 input dimensions can improve the performance of other algorithms afterward (see the third
 170 row of Fig. [Figure 2](#)).

171 This module relies on the *scikit-learn* library, which provides access to a wide range of
 172 algorithms (25 at the time of writing). As a result, all algorithms available in the *scikit-learn*
 173 decomposition and cluster modules that have common APIs (namely, a `fit()`, a
 174 `transform()`, or a `fit_transform()` method) can be used. Note that the UMAP approach
 175 relies instead on its dedicated Python implementation and is an optional dependency at the
 176 time of writing.

177 Unsupervised clustering

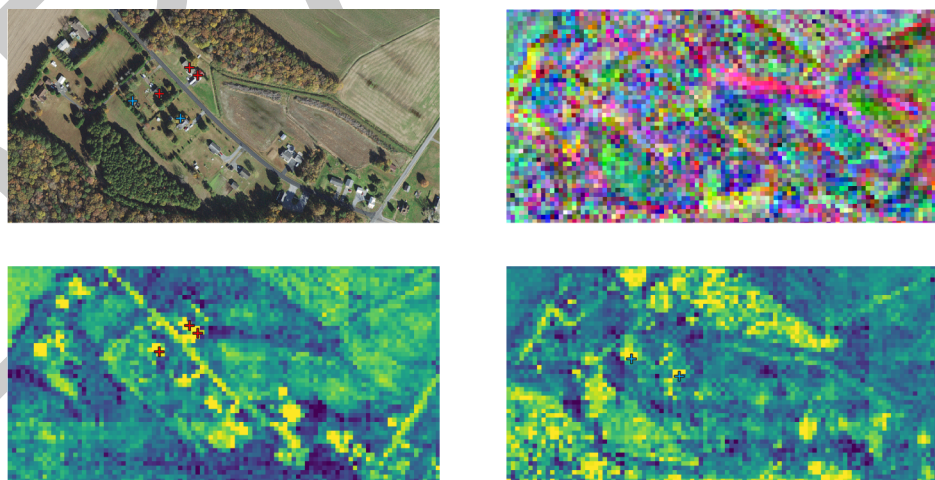
178 A common operation when handling feature spaces is clustering to assign classes to data
 179 points. The unsupervised clustering module allows to implement various unsupervised clustering
 180 algorithms, including K-means or HDBSCAN (McInnes et al., 2017) (see Fig. Figure 3). This
 181 module again relies on *scikit-learn* as a back-end. As such, all algorithms available in the
 182 *scikit-learn* cluster module sharing common APIs (namely, a `fit()`, a `predict()`, or a
 183 `fit_predict()` method) can be used.



184 **Figure 3:** Example of different clustering ($k=5$) of the ViT Base DINO features.

184 Similarity approach

185 When exploring high-dimensional spaces, similarity search is a common task. The similarity
 186 approach module of IAMAP enables users to generate similarity maps based on one or more
 187 point shapefiles. This module relies on cosine similarity, which assigns a score between 0 and 1
 188 to two points based on their coordinates in the feature space. The score is zero if the vectors
 189 represented by these coordinates are orthogonal to the reference vectors provided by the user,
 190 and 1 if they are identical. This approach is commonly used for instance retrieval tasks in
 191 deep learning (Chen et al., 2022), as it helps identify points that are closely represented in the
 192 feature space (see Fig. Figure 4 for examples). By applying a threshold, this method can also
 193 be used for simple segmentation tasks.



184 **Figure 4:** Example usage of cosine similarity with [NAIP data](#). Using only a couple of points, we can
 185 identify trees or houses without needing to train a model for this specific task. From left to right and top
 186 to bottom: Original RGB data and provided template points (red and blue crosses); Features produced
 187 by a ViT DINO small encoder (Caron et al., 2021); Heatmap produced with the red points as input
 188 (houses); Heatmap produced with the blue points as input (trees with red leaves).

194 Supervised machine learning

195 The final module of IAMAP enables users to build supervised predictive models using classical
196 machine learning algorithms such as Random Forests, KNN, or Gradient Boosting. In contrast
197 to other plugins that enable the use of end-to-end deep learning models for specific tasks (e.g.
198 [Aszkowski et al., 2023](#)), we have focused on lighter machine learning algorithms to minimize
199 dataset and computational resource requirements. These algorithms often require relevant
200 input features to be able to perform. While deep learning is now more potent on a lot of tasks,
201 ML algorithms used with deep learning features as input can achieve satisfactory performances
202 with a fraction of the cost needed to fit the algorithm. Then for example, algorithms such as
203 KNN are used in deep learning research to evaluate models trained in an unsupervised way
204 without having to retrain an entire model (e.g. see SM of [\(Caron et al., 2021\)](#)).

205 The plugin provides a wide array of available algorithms, once again using the *scikit-learn*
206 library as a back-end. More specifically, all methods provided by the ensemble and neighbors
207 modules that share a common API are available.

208 Because this module relies on supervised approaches, it requires the user to provide a reference
209 point dataset as a shapefile. The sampling design of this reference dataset is left to the user
210 but we provide the option to choose how the validation scheme is performed. By default, a
211 cross validation in k-fold is performed by randomly splitting the dataset into 5 folds. Otherwise,
212 it is possible to define the train/test split or the cross-validation scheme dataset according to
213 the values in a attribute column. As the appropriate validation scheme depends largely on the
214 dataset and target task, this validation scheme might not be the most appropriate (see [\(Ploton
215 et al., 2020\)](#) for discussion on this topic in the context of spatial datasets). We therefore
216 encourage the users to consider their choices of validation scheme via the plugin interface.

217 Usage example

218 Because the IAMAP plugin consists of a set of different modules that can be implemented
219 independently or sequentially in various combinations, the number of possible uses is very
220 large. Here, we provide one example of a potential workflow to produce a classification map
221 using three complementary IAMAP modules (Fig.[Figure 5](#)). Several other use cases, along
222 with detailed protocols, are available [in the online documentation of the plugin](#).

An example of workflow implemented using IAMAP to produce a ca. 50-m classification map
from a 10-m multispectral Sentinel 2 image over a forested landscape from Thailand (Lat
7.53°, Lon 99.82°).

Figure 5: An example of workflow implemented using IAMAP to produce a ca. 50-m classification map
from a 10-m multispectral Sentinel 2 image over a forested landscape from Thailand (Lat 7.53°, Lon
99.82°).

223 Design choices

224 We have aimed the development for the plugin to be usable on a laptop without a GPU by
225 someone with no coding experience. This has come with various design choices.

226 Cross-platform and easy to install

227 The plugin is designed to be easy to install, especially working with state of the art deep learning
228 dependencies. Dependencies are handled using *pip* with a startup script that automatically
229 looks for dependencies and installs the missing one if needed. If needed, a *conda* environment
230 formula is provided as well to work in a separate fixed environment. The plugin has been tested
231 on Windows, Mac and Linux with several QGIS versions. Although the plugin does not require

232 a GPU to function, if one is detected, the correct version of *pytorch* is downloaded to be used
233 during deep learning inference. The user may opt out the usage of the GPU afterwards.

234 **Inference as a stoppable background task**

235 The inference of deep learning models on large raster images may be long, in particular without
236 a GPU. Then, we have given the option to schedule small pauses during the inference, which
237 limits the CPU usage and enables to use the PC for other tasks during the inference. An other
238 choice has been to save batches on disk rather than keeping all inferred tiles on RAM. While
239 slower, this makes possible to stop the inference and start again latter (even after reboot).
240 Temporary files are cleaned up after use.

241 The produced rasters can become heavy and are therefore compressed by default to save space.

242 **Model quantization**

243 The quantization of a deep learning model is the act of switching the encoding of the weights
244 from *float32* to a lighter format such as *uint8*. This greatly reduces model size and inference
245 time, at the cost of some precision (see [pytorch documentation](#)) ([Wu et al., 2020](#)). Recently,
246 DeepSeek AI have been able to divide training costs by 40 by relying on similar methods with
247 *fp8* precision training ([Liu et al., 2024](#)). This practice is common when working with hardware
248 size constraints. Here, we give the option to the user to quantize the model before inference.
249 When working with a model that was not specifically trained for the task asked of it, the
250 trade-off between speed and precision could be beneficial more often than not.

251 **Perspectives and future developments**

252 **Limitations of the plugin**

253 This plugin is though for a usage in conditions where the end-to-end training of a neural
254 network is not a possibility because of a lack of data or computing power. This comes with
255 limitations to what is possible with deep learning in inference only compared to what can be
256 achieved with neural network trained classically.

257 First, some task will require non-linear and complex connections in the feature space and will
258 not be possible with simple manipulations as those possible with this plugin. For example,
259 complex tasks as instance segmentation is easily achievable with dedicated deep learning
260 models (see ([Zhao et al., 2023](#))) but not with our plugin.

261 By using deep learning methods, classical machine learning and data manipulation methods,
262 this plugin inherits from advantages but also drawbacks from different types of algorithms.
263 Ideally and depending on the use case, the use of a deep learning encoder will provide relevant
264 features, robust to low level noise and transformations. These features can then be leveraged
265 with lighter machine learning algorithms, enabling the creation of maps that would not be
266 possible without the features provided by a deep learning encoder. On the other hand, it may
267 be required to test a variety of encoders and hyper-parameters to achieve satisfying results.
268 While projection or clustering techniques are often easy to fit, testing different deep learning
269 models can be time consuming, especially on restricted hardware.

270 **Future developments**

271 Future developments for the plugin include keeping up with computer vision state of the art
272 but also optimization techniques to ensure lightweight inference time and usability on restricted
273 hardware.

274 Moreover, we aim to implement more models dedicated to remote sensing tasks (for instance,
275 those evaluated by ([Marsocci et al., 2024](#))). As of now, the feature extraction tool is though

276 for ViT like encoders, that have spatially explicit features. We aim to develop it to be more
277 generalist and take any encoder as input, such as ResNets or UNets that are still widely used
278 in deep learning and remote sensing.

279 Availability

280 Development of the plugin is [open sourced on GitHub](#). Documentation is available [on](#)
281 [readthedocs](#). The plugin is developed in continuous integration. We plan to publish the plugin
282 on official QGIS repository to further ease the installation process.

283 Acknowledgments

284 The authors would like to thank all people who have tested this software during development
285 and have provided meaningful feedback.

286 Conflict of interest

287 The authors declare no conflict of interest.

288 References

- 289 Achiam, J., Adler, S., Agarwal, S., Ahmad, L., Akkaya, I., Aleman, F. L., Almeida, D.,
290 Altenschmidt, J., Altman, S., Anadkat, S., & others. (2023). Gpt-4 technical report. *arXiv*
291 *Preprint arXiv:2303.08774*.
- 292 Aszkowski, P., Ptak, B., Kraft, M., Pieczyński, D., & Drapikowski, P. (2023). Deepness: Deep
293 neural remote sensing plugin for QGIS. *SoftwareX*, 23, 101495. <https://doi.org/https://doi.org/10.1016/j.softx.2023.101495>
- 295 Bardes, A., Ponce, J., & LeCun, Y. (2021). Vicreg: Variance-invariance-covariance regulariza-
296 tion for self-supervised learning. *arXiv Preprint arXiv:2105.04906*.
- 297 Caron, M., Touvron, H., Misra, I., Jégou, H., Mairal, J., Bojanowski, P., & Joulin, A. (2021).
298 Emerging properties in self-supervised vision transformers. *Proceedings of the International
299 Conference on Computer Vision (ICCV)*, 9650–9660.
- 300 Chen, W., Liu, Y., Wang, W., Bakker, E. M., Georgiou, T., Fieguth, P., Liu, L., & Lew, M.
301 S. (2022). Deep learning for instance retrieval: A survey. *IEEE Transactions on Pattern
302 Analysis and Machine Intelligence*, 45(6), 7270–7292.
- 303 Cong, Y., Khanna, S., Meng, C., Liu, P., Rozi, E., He, Y., Burke, M., Lobell, D. B., & Ermon,
304 S. (2023). SatMAE: Pre-training transformers for temporal and multi-spectral satellite
305 imagery. <https://arxiv.org/abs/2207.08051>
- 306 Devlin, J. (2018). Bert: Pre-training of deep bidirectional transformers for language under-
307 standing. *arXiv Preprint arXiv:1810.04805*.
- 308 Dosovitskiy, A., Beyer, L., Kolesnikov, A., Weissenborn, D., Zhai, X., Unterthiner, T., Dehghani,
309 M., Minderer, M., Heigold, G., Gelly, S., & others. (2020). An image is worth 16x16 words:
310 Transformers for image recognition at scale. *arXiv Preprint arXiv:2010.11929*.
- 311 Ericsson, L., Gouk, H., & Hospedales, T. M. (2021). How well do self-supervised models
312 transfer? *Proceedings of the IEEE/CVF Conference on Computer Vision and Pattern
313 Recognition*, 5414–5423.
- 314 Fang, Y., Wang, W., Xie, B., Sun, Q., Wu, L., Wang, X., Huang, T., Wang, X., & Cao,
315 Y. (2023). Eva: Exploring the limits of masked visual representation learning at scale.

- 316 *Proceedings of the IEEE/CVF Conference on Computer Vision and Pattern Recognition*,
 317 19358–19369.
- 318 Goodfellow, I. (2016). *Deep learning*. MIT press.
- 319 He, K., Chen, X., Xie, S., Li, Y., Dollár, P., & Girshick, R. (2022). Masked autoencoders are
 320 scalable vision learners. *Proceedings of the IEEE/CVF Conference on Computer Vision*
 321 and *Pattern Recognition*, 16000–16009.
- 322 Jakubik, J., Roy, S., Phillips, C. E., Fraccaro, P., Godwin, D., Zadrožny, B., Szwarcman, D.,
 323 Gomes, C., Nyirjesy, G., Edwards, B., Kimura, D., Simumba, N., Chu, L., Mukkavilli, S.,
 324 K., Lambhate, D., Das, K., Bangalore, R., Oliveira, D., Muszynski, M., ... Ramachandran,
 325 R. (2023). Foundation Models for Generalist Geospatial Artificial Intelligence. *Preprint*
 326 Available on Arxiv:2310.18660.
- 327 Liu, A., Feng, B., Xue, B., Wang, B., Wu, B., Lu, C., Zhao, C., Deng, C., Zhang, C., Ruan,
 328 C., & others. (2024). Deepseek-v3 technical report. *arXiv Preprint arXiv:2412.19437*.
- 329 Marsocci, V., Jia, Y., Bellier, G. L., Kerekes, D., Zeng, L., Hafner, S., Gerard, S., Brune, E.,
 330 Yadav, R., Shibli, A., Fang, H., Ban, Y., Vergauwen, M., Audebert, N., & Naselli, A.
 331 (2024). PANGAEA: A global and inclusive benchmark for geospatial foundation models.
 332 <https://arxiv.org/abs/2412.04204>
- 333 McInnes, L., Healy, J., Astels, S., & others. (2017). Hdbscan: Hierarchical density based
 334 clustering. *J. Open Source Softw.*, 2(11), 205.
- 335 McInnes, L., Healy, J., & Melville, J. (2018). Umap: Uniform manifold approximation and
 336 projection for dimension reduction. *arXiv Preprint arXiv:1802.03426*.
- 337 Oquab, M., Darabet, T., Moutakanni, T., Vo, H., Szafraniec, M., Khalidov, V., Fernandez, P.,
 338 Haziza, D., Massa, F., El-Nouby, A., & others. (2023). Dinov2: Learning robust visual
 339 features without supervision. *arXiv Preprint arXiv:2304.07193*.
- 340 Ploton, P., Mortier, F., Réjou-Méchain, M., Barbier, N., Picard, N., Rossi, V., Dormann, C.,
 341 Cornu, G., Viennois, G., Bayol, N., & others. (2020). Spatial validation reveals poor
 342 predictive performance of large-scale ecological mapping models. *Nature Communications*,
 343 11(1), 4540.
- 344 QGIS Development Team. (2025). *QGIS geographic information system*. Open Source
 345 Geospatial Foundation. <http://qgis.org>
- 346 Ryali, C., Hu, Y.-T., Bolya, D., Wei, C., Fan, H., Huang, P.-Y., Aggarwal, V., Chowdhury,
 347 A., Poursaeed, O., Hoffman, J., Malik, J., Li, Y., & Feichtenhofer, C. (2023). Hiera: A
 348 hierarchical vision transformer without the bells-and-whistles. *ICML*.
- 349 Safonova, A., Ghazaryan, G., Stiller, S., Main-Knorn, M., Nendel, C., & Ryo, M. (2023). Ten
 350 deep learning techniques to address small data problems with remote sensing. *International*
 351 *Journal of Applied Earth Observation and Geoinformation*, 125, 103569.
- 352 Shwartz Ziv, R., & LeCun, Y. (2024). To compress or not to compress—self-supervised learning
 353 and information theory: A review. *Entropy*, 26(3), 252.
- 354 Stewart, A. J., Robinson, C., Corley, I. A., Ortiz, A., Lavista Ferres, J. M., & Banerjee,
 355 A. (2022). TorchGeo: Deep learning with geospatial data. *Proceedings of the 30th*
 356 *International Conference on Advances in Geographic Information Systems*, 1–12. <https://doi.org/10.1145/3557915.3560953>
- 358 Van der Maaten, L., & Hinton, G. (2008). Visualizing data using t-SNE. *Journal of Machine*
 359 *Learning Research*, 9(11).
- 360 Vaswani, A. (2017). Attention is all you need. *Advances in Neural Information Processing*
 361 *Systems*.

- 362 Wang, Y., Braham, N. A. A., Xiong, Z., Liu, C., Albrecht, C. M., & Zhu, X. X. (2022).
363 SSL4EO-S12: A large-scale multi-modal, multi-temporal dataset for self-supervised learning
364 in earth observation. *arXiv Preprint arXiv:2211.07044*.
- 365 Wightman, R. (2019). PyTorch image models. In *GitHub repository*. <https://github.com/rwightman/pytorch-image-models>; GitHub. <https://doi.org/10.5281/zenodo.4414861>
- 366 Wolf, T. (2019). Huggingface's transformers: State-of-the-art natural language processing.
368 *arXiv Preprint arXiv:1910.03771*.
- 369 Wu, H., Judd, P., Zhang, X., Isaev, M., & Micikevicius, P. (2020). Integer quantization for deep
370 learning inference: Principles and empirical evaluation. *arXiv Preprint arXiv:2004.09602*.
- 371 Xiong, Z., Wang, Y., Zhang, F., Stewart, A. J., Hanna, J., Borth, D., Papoutsis, I., Saux, B.
372 L., Camps-Valls, G., & Zhu, X. X. (2024). Neural plasticity-inspired foundation model for
373 observing the Earth crossing modalities. *arXiv Preprint arXiv:2403.15356*.
- 374 Yasir, M., Jianhua, W., Shanwei, L., Sheng, H., Mingming, X., & Hossain, M. (2023).
375 Coupling of deep learning and remote sensing: A comprehensive systematic literature
376 review. *International Journal of Remote Sensing*, 44(1), 157–193.
- 377 Yuan, Q., Shen, H., Li, T., Li, Z., Li, S., Jiang, Y., Xu, H., Tan, W., Yang, Q., Wang, J.,
378 & others. (2020). Deep learning in environmental remote sensing: Achievements and
379 challenges. *Remote Sensing of Environment*, 241, 111716.
- 380 Zhao, Z., Fan, C., & Liu, L. (2023). *Geo SAM: A QGIS plugin using Segment Anything
381 Model (SAM) to accelerate geospatial image segmentation* (Version 1.1.0). Zenodo.
382 <https://doi.org/10.5281/zenodo.8191039>
- 383 Zhu, X. X., Tuia, D., Mou, L., Xia, G.-S., Zhang, L., Xu, F., & Fraundorfer, F. (2017). Deep
384 learning in remote sensing: A comprehensive review and list of resources. *IEEE Geoscience
385 and Remote Sensing Magazine*, 5(4), 8–36.